

# A dynamic mode decomposition extension for the forecasting of parametric dynamical systems

Francesco Andreuzzi\*, Nicola Demo† and Gianluigi Rozza‡

Mathematics Area, mathLab, SISSA, via Bonomea 265, I-34136 Trieste, Italy

October 19, 2021

## Abstract

Dynamic mode decomposition (DMD) has recently become a popular tool for the non-intrusive analysis of dynamical systems. Exploiting the proper orthogonal decomposition as dimensionality reduction technique, DMD is able to approximate a dynamical system as a sum of (spatial) basis evolving linearly in time, allowing for a better understanding of the physical phenomena or for a future forecasting. We propose in this contribution an extension of the DMD to parametrized dynamical systems, focusing on the future forecasting of the output of interest in a parametric context. Initially, all the snapshots — for different parameters and different time instants — are projected to the reduced space, employing the DMD (or one of its variants) to approximate the reduced snapshots for a future instants. Still exploiting the low dimension of the reduced space, the predicted reduced snapshots are then combined using a regression technique, enabling the possibility to approximate any untested parametric configuration in any future instant. We are going to present here the algorithmic core of the aforementioned method, presenting at the end three different test cases with incremental complexity: a simple dynamical system with a linear parameter dependency, a heat problem with nonlinear parameter dependency and a fluid dynamics problem with nonlinear parameter dependency.

## 1 Introduction

Several applications in the computational sciences field require an iterative or real-time evaluation of the mathematical model in hand. In these contexts, reduced order modeling (ROM) allows for an efficient performing of the aforementioned tasks by reducing the dimensionality of the original model. Dynamic mode decomposition (DMD) [12] has gained popularity in last years as ROM for dynamical systems, being successfully applied to fluid dynamics problems [21, 20, 19]. Such technique performs a model simplification in a data-driven fashion, and is able to individuate the main structures of the original problem and then predict the system state in future. However, in many applications it becomes fundamental to study not only the dynamics of the system, but also its dependency on some parameters. For practical examples, the reader can think of the position of the source in an unsteady heat problem or the fluid velocity in a computational fluid dynamics one.

Parametric time-dependent problem can be treated in a projection framework exploiting proper orthogonal decomposition (POD) [4, 7] for dimensionality reduction. Such approach requires — due to projection step — the knowledge of the original model, as well as the access to the discrete operators of the problem. Concerning the non-intrusive methodologies instead, one approach proposed in [8] consists in the extraction of the main spatio-temporal structure to isolate the parameter dependency. This technique is not able to predict the output of the system for a future time steps, but provides the reconstruction of the parametric manifold. A preliminary approach for future forecast of parametric system is presented in [21], consisting in an application of DMD

---

\*francesco.andreuzzi@sissa.it

†nicola.demo@sissa.it

‡gianluigi.rozza@sissa.it

to parameter-dependent scalar output in order to predict such output for untested parameters and time steps.

In this work we propose an extension of the latter approach in order to predict not only scalar output but also the entire discrete fields. A parametric version of DMD has been already studied in [18], but the intent of that work is the extraction of coherent structures shared between different configuration of the system. To the best of the authors knowledge, an approach for predicting the fields of interest for unseen time instants and parameters is not explored in literature yet.

Following the standard DMD method, our extension takes in input an initial dataset composed by the high-fidelity snapshots, equispaced in time and for different parametric configurations. Such snapshots are then reduced in dimensionality through a POD approach and re-arranged in order to feed the DMD algorithm. In this sense, the DMD is applied in order to forecast the reduced snapshots in future. After this step we have the predicted reduced snapshots for all the parametric points which compose the initial dataset. Then, the parametric manifold can be reconstructed using an approach similar to PODI [1, 3, 20] by involving a regression technique to approximate the mapping between parameters and the (forecasted) reduced snapshots. Since this technique works on a reduced space, the computational cost for any new evaluations is small with respect to traditional discretization methods, e.g. finite element and finite volume. We remark also that the ROM is equation-agnostic, since it relies only on the high-fidelity snapshots and not requiring information about the original model.

The present contribution is organised as follows: in section 2 we initially introduce the original DMD formulation and its higher order variant, to make easier the comprehension of the parametric approach we propose in section 2.3. In section 3 we present numerical results obtained on three problems with heterogeneous parametric dependency. Finally we discuss some possible future developments.

## 2 Methods

We dedicate this section to a brief introduction about DMD and its higher order variant which we are going to exploit in some cases for the parametric approach. After that, we are going to introduce our parametric extension of DMD, for which we consider two variants.

### 2.1 Dynamic Mode Decomposition

DMD is a data driven method for the analysis of dynamical systems. We provide a brief introduction to the general technique in order to make the extension described in section 2 more clear to the reader.

We consider a time-dependent vector function  $\mathbf{x}_k \in \mathbb{R}^m$ . The function  $\mathbf{x}_k$  may evolve in a discrete set of time instants  $(\mathbf{x}_1, \mathbf{x}_2, \dots)$ , or more generally it may be the result of a sampling. We are going to call each  $\mathbf{x}_k$  a *snapshot* of the vector quantity of interest. Given a snapshot  $\mathbf{x}_k$  we consider  $\mathbf{x}_{k+1}$  to be the subsequent snapshot. We seek an operator  $\mathbf{A} \in \mathbb{R}^{m \times m}$  such that:

$$\mathbf{x}_{k+1} = \mathbf{A}\mathbf{x}_k. \quad (2.1)$$

The operator  $\mathbf{A}$  can be considered a finite approximation of the *Koopman operator* [11], which is infinite-dimensional. In order to build such operator satisfying eq. (2.1) up to an acceptable degree of approximation, we consider a set  $\mathcal{T}$  of discrete time instants equispaced in time, which we are going to refer to as *tested time instants*, or *known time instants* in the following paragraphs. For the sake of simplicity we are going to name these time instants using the labels  $\{1, \dots, N\}$ . We remark that we do not specify any relation between the label of the time instants and the time (in seconds) when a snapshot is collected. This relation must be specified in the formulation of the problem, we intend to remain general in this section. Then, we obtain  $N$  snapshots of the function of interests  $\{\mathbf{x}_1, \dots, \mathbf{x}_N\}$ , which are to be used during the training phase of DMD. We arrange the snapshots in two matrices  $\mathbf{X}, \mathbf{Y} \in \mathbb{R}^{m \times N-1}$  defined as follows:

$$\mathbf{X} = [\mathbf{x}_1, \mathbf{x}_2, \dots, \mathbf{x}_{N-1}], \quad \mathbf{Y} = [\mathbf{x}_2, \mathbf{x}_3, \dots, \mathbf{x}_N]. \quad (2.2)$$

We now attempt to find the matrix  $\mathbf{A}$  such that  $\mathbf{Y} \approx \mathbf{A}\mathbf{X}$  (note that such an operator satisfies the condition eq. (2.1)  $\forall k \in \{1, \dots, N-1\}$ ). Denoting the Moore-Penrose pseudo-inverse operator

by  $\dagger$ , we can find the best-fit operator  $\mathbf{A} = \mathbf{Y}\mathbf{X}^\dagger$  [16]. However this computation is expensive and generally intractable, therefore we follow another path.

Consider the  $r$ -ranked singular value decomposition of  $\mathbf{X} \approx \mathbf{U}_r \mathbf{\Sigma}_r \mathbf{V}_r^*$  [17]. Since the matrix  $\mathbf{U}_r$  is orthogonal, we take the low-rank projection  $\tilde{\mathbf{A}} \in \mathbb{R}^{r \times r}$  of the operator  $\mathbf{A}$  onto the subspace spanned by the columns of  $\mathbf{U}_r$ :

$$\tilde{\mathbf{A}} = \mathbf{U}_r^* \mathbf{A} \mathbf{U}_r = \mathbf{U}_r^* \mathbf{Y} \mathbf{X}^\dagger \mathbf{U}_r = \mathbf{U}_r^* \mathbf{Y} \mathbf{V}_r \mathbf{\Sigma}_r^{-1} \mathbf{U}_r^* \mathbf{U}_r = \mathbf{U}_r^* \mathbf{Y} \mathbf{V}_r \mathbf{\Sigma}_r^{-1}. \quad (2.3)$$

Note that this computation does not involve the evaluation of the unprojected operator  $\mathbf{A}$ . It can be shown that the eigenvalues of  $\mathbf{A}$  are the same of  $\tilde{\mathbf{A}}$ , and that the eigenvectors of the full operator are obtained from those of the low-rank one [12]. Since the eigendecomposition of the low-rank operator involves a tractable computation due to the low dimensionality of the matrix  $\tilde{\mathbf{A}}$ , we obtained the eigendecomposition of  $\mathbf{A}$  through the manipulations of low-rank matrices.

Denoting by  $\Phi \in \mathbb{R}^{m \times r}$  the matrix of the eigenvectors of  $\mathbf{A}$ , and by  $\Lambda \in \mathbb{R}^{r \times r}$  the diagonal matrix of its eigenvalues, it can be shown that:

$$\mathbf{x}_k = \Phi \Lambda^k \Phi^\dagger \mathbf{x}_1. \quad (2.4)$$

There are virtually no constraints on  $k \in \mathbb{N}$ , therefore it is possible to use eq. (2.4) to approximate the value of  $\mathbf{x}_k$  for  $k > N$ , namely we can predict the behavior of the function of interest in future time instants. We are going to use this feature in section 2 in order to expand the known time frame.

## 2.2 Higher-Order Dynamic Mode Decomposition

The quality of results obtained using DMD might decay if  $m \approx N$  [13], where  $m$  is the space dimension (the number of components of the vector function of interest) and  $N$  is the number of time instants considered during the training phase. It has been observed that the situation becomes even worse when  $m < N$ . A possible solution to this problem is given by Higher Order Dynamic Mode Decomposition (HODMD), a variant of DMD which is able to extract more significative modes from low-dimensional data [13].

The key part of this variant is the replacement of the usual expression  $x_{k+1} \approx A x_k$  with the following expression, which uses  $d$  time lagged snapshots (this is usually called *higher order Koopman assumption*):

$$\mathbf{x}_{k+d} = \mathbf{A}_1 \mathbf{x}_k + \mathbf{A}_2 \mathbf{x}_{k+1} + \dots + \mathbf{A}_d \mathbf{x}_{k+d-1}. \quad (2.5)$$

If we set  $\bar{\mathbf{x}}_k := [\mathbf{x}_k, \mathbf{x}_{k+1}, \dots, \mathbf{x}_{k+d-1}]^\top$  we may rewrite eq. (2.5) in a compact form which resembles eq. (2.1):  $\bar{\mathbf{x}}_{k+1} = \mathbf{A} \bar{\mathbf{x}}_k$ . In fact this form allows us to find an approximation of the operator  $\mathbf{A}$  like we did in section 2.1. Experimental results show that this approach produces better results in several situations [15, 14].

HODMD is a useful addition for our approach, since we usually consider a significant dimensionality reduction before the application of DMD (this is a compulsory step because the interpolation would be unfeasible from a computational perspective otherwise). To fix the results provided by DMD, whose quality is usually reduced by the reduction, we may use HODMD instead.

## 2.3 Dynamic Mode Decomposition for parametric problems

In this section we propose a possible application of DMD to a parametrized dynamical system. The parameter belongs to a generic set  $\mathbb{P}$ , which we refer to as *parameters set*. Considering a discrete space, we define the output of interest as the vector function  $\mathbf{x}_k^\mu \in \mathbb{R}^m$ , which depends on the parameter  $\mu \in \mathbb{P}$  and on the time instant  $k$ .

As in the original formulation, we initially collect a set of  $N$  high-fidelity snapshots of the system with a fixed parameter at equispaced time instants. We recall that  $\mathcal{T}$  is the set of time instants used during the training phase, we keep using the labeling of time instants introduced in section 2.1, namely  $\mathcal{T} = \{1, \dots, N\}$ . We also consider  $p$  parameters, which we collect into the *training set*  $\mathcal{S} = \{\mu_1, \dots, \mu_p\}$ , and we replicate the previous step  $p$  times, one for each parametric sample. We obtain then  $p$  parametric configurations, each one containing  $N$  time instants, overall  $p \times N$  snapshots. The basic idea is then to apply a POD-based reduction to the snapshots in order to obtain their reduced representation, also referred in literature as modal coefficients or

reduced snapshots [6]. Then we apply DMD in order to approximate reduced snapshots in future time instants [12]: this allows to explore the solution manifold using some regression techniques [1] in future time instants, approximating the relation between parameters and reduced snapshots. Finally the interpolated reduced snapshot is mapped back to the full-dimensional space.

During the numerical experiments we consider two different approaches for the application of DMD to the reduced snapshots. In the first case, we build a unique linear operator to fit the dynamics of the entire (parametrized) system. Alternatively,  $p$  linear operators are constructed to approximate the dynamics of the  $p$  parametric configurations. In the next subsections, we formally define these two approaches, referred from now on as *monolithic* and *partitioned*, presenting also the regression technique and some numerical stabilization we impose on DMD operator for more robust forecasting.

### 2.3.1 Monolithic approach

We consider  $p$  matrices  $\mathbf{X}^{\mu_i}$  (one for each parameter in the training set  $\mathcal{S} = \{\mu_1, \dots, \mu_p\}$ ) and the matrix  $\mathcal{X}_1$  defined as follows:

$$\mathbf{X}^{\mu_i} := \begin{bmatrix} | & \cdots & | \\ \mathbf{x}_1^{\mu_i} & \cdots & \mathbf{x}_N^{\mu_i} \\ | & \cdots & | \end{bmatrix} \in \mathbb{R}^{m \times N}, \quad \mathcal{X}_1 := [\mathbf{X}^{\mu_1} \dots \mathbf{X}^{\mu_p}] \in \mathbb{R}^{m \times Np}. \quad (2.6)$$

Note that the columns of each  $\mathbf{X}^{\mu_i}$  are the (sampled) evolution over time of the vector function  $\mathbf{x}_k^{\mu_i} \in \mathbb{R}^m$ , in the time instants belonging to the set  $\mathcal{T}$ . We apply POD to the matrix  $\mathcal{X}_1$  to obtain the optimal<sup>1</sup> space of dimension  $n$  to represent all the original snapshots, with  $0 < n \leq \min(m, Np)$ . POD method returns indeed the matrix  $\mathbf{U}_n \in \mathbb{R}^{m \times n}$  which contains the reduced space basis, or POD modes [6]. The number  $n$  of retained POD modes is selected by the user, and must be selected carefully since it affects the quality of the results provided by the algorithm. A small value may result in a low-quality reconstruction of the output function, since important spacial informations may have been discarded; an high value may increase the computational cost of the online phase, as well as increase the error introduced by regressors due to the higher dimension.

We can exploit the matrix  $\mathbf{U}_n$  to compute the modal coefficients corresponding to the snapshots stored in the columns of the matrix  $\mathcal{X}_1$ : in matrix form we have  $\tilde{\mathbf{X}} = \mathbf{U}_n^* \mathcal{X}_1 \in \mathbb{R}^{n \times Np}$ . The columns of  $\tilde{\mathbf{X}}$  are the reduced snapshots which we mentioned earlier. We refer by  $\tilde{\mathbf{x}}_k^{\mu_i} := \mathbf{U}_n^* \mathbf{x}_k^{\mu_i} \in \mathbb{R}^n$  to the vector of POD coefficients corresponding to the  $k$ -th snapshot of the system with parameter  $\mu_i$ . Note that POD coefficients evolve in time, therefore we would like to predict this evolution in future time instants in order to obtain the full-dimensional counterpart of the snapshot, which we could later use to explore the solution manifold.

In order to employ the DMD method introduced in section 2.1 we arrange POD coefficients in the following way:

$$\tilde{\mathbf{X}}^{\mu_i} := \mathbf{U}_n^* \mathbf{X}^{\mu_i} = \begin{bmatrix} | & \cdots & | \\ \tilde{\mathbf{x}}_1^{\mu_i} & \cdots & \tilde{\mathbf{x}}_N^{\mu_i} \\ | & \cdots & | \end{bmatrix} \in \mathbb{R}^{n \times N}, \quad \mathcal{X}_2 := \begin{bmatrix} \tilde{\mathbf{X}}^{\mu_1} \\ \tilde{\mathbf{X}}^{\mu_2} \\ \vdots \\ \tilde{\mathbf{X}}^{\mu_p} \end{bmatrix} \in \mathbb{R}^{np \times N}. \quad (2.7)$$

Each matrix  $\tilde{\mathbf{X}}^{\mu_i}$  is the reduced representation (in the POD subspace) of the corresponding matrix  $\mathbf{X}^{\mu_i}$ , and is obtained with a single matrix multiplication with POD modes. At this point we apply DMD to the matrix  $\mathcal{X}_2$ , whose columns are temporal snapshots representing different realizations of the parametric system. Arranging these columns in two matrices,  $\mathcal{X}_2^1 \in \mathbb{R}^{np \times (N-1)}$  and  $\mathcal{X}_2^2 \in \mathbb{R}^{np \times (N-1)}$ , we recall that the DMD operator is the matrix  $\tilde{\mathbf{A}}$  such that  $\mathcal{X}_2^2 = \tilde{\mathbf{A}} \mathcal{X}_2^1$  as we stated in section 2.1. We note that, since in our method the dimension reduction is employed at the beginning, the typical compression step performed in the standard DMD formulation (eq. (2.3)) might not be needed, depending by the number of parametric samples. In the case, the DMD operator can be found using just the least-square procedure.

As we mentioned the DMD operator  $\tilde{\mathbf{A}}$  can be used to advance a vector of reduced snapshots

---

<sup>1</sup>in linear sense

by one time instant:

$$\begin{bmatrix} \tilde{\mathbf{x}}_{k+1}^{\mu_1} \\ \vdots \\ \tilde{\mathbf{x}}_{k+1}^{\mu_p} \end{bmatrix} = \tilde{\mathbf{A}} \begin{bmatrix} \tilde{\mathbf{x}}_k^{\mu_1} \\ \vdots \\ \tilde{\mathbf{x}}_k^{\mu_p} \end{bmatrix} \in \mathbb{R}^{np}$$

It might not be formally correct to keep using the notation  $\tilde{\mathbf{x}}_k^{\mu_i}$  when  $k > N$ , since in this case the vector is an approximation of the reduced snapshot computed using DMD and eq. (2.4). However we are going to use the same notation to avoid introducing another one for predicted reduced snapshots. We do this without ambiguity, since in this work we are not going to consider reduced snapshots for  $k > N$ .

We rewrite the last equation using the notation adopted, and we also replace the generic  $k$  with the first time instant of interest for our discussion, namely the last one:

$$\begin{bmatrix} \tilde{\mathbf{x}}_{N+1}^{\mu_1} \\ \vdots \\ \tilde{\mathbf{x}}_{N+1}^{\mu_p} \end{bmatrix} = \tilde{\mathbf{A}} \begin{bmatrix} \tilde{\mathbf{x}}_N^{\mu_1} \\ \vdots \\ \tilde{\mathbf{x}}_N^{\mu_p} \end{bmatrix} \in \mathbb{R}^{np} \quad (2.8)$$

---

**Algorithm 1** Dynamic Mode Decomposition for parametric problems — Monolithic

---

**Input:**  $\mathbf{X}^{\mu_1}, \dots, \mathbf{X}^{\mu_p} \in \mathbb{R}^{m \times N}$

Construct the matrix  $\mathcal{X}_1 \in \mathbb{R}^{m \times Np}$   
 Compute the POD coefficients of the columns of  $\mathcal{X}_1$   
 Store the coefficients into  $\tilde{\mathbf{X}}^{\mu_i}, i \in \{1, \dots, p\}$   
 Construct the matrix  $\mathcal{X}_2 \in \mathbb{R}^{np \times N}$   
 Compute the DMD operator  $\tilde{\mathbf{A}}$  by fitting  $\mathcal{X}_2$

---

We remark that the monolithic approach relies on a unique DMD operator to express the dynamics of the parametric system. This implies that the operator is able to detect recurrent patterns in the dynamics of different parametric configurations, making its usage particular profitable when the different realizations share common behaviours.

### 2.3.2 Partitioned approach

We considered also another similar approach, inspired by the observation of patterns extracted with DMD as shown in section 2.3.1 for particular dynamical systems. We are going to use the same notation, when possible, introduced in section 2.3.1.

Starting from the  $p$  matrices  $\mathbf{X}^{\mu_i}$  we construct  $\mathcal{X}_1$  as in eq. (2.6). Then we apply POD to  $\mathcal{X}_1$  to obtain POD modes  $\mathbf{U}_n \in \mathbb{R}^{m \times n}$ , and we compute modal coefficients  $\tilde{\mathbf{X}}^{\mu_i} = \mathbf{U}_n^\top \mathbf{X}^{\mu_i}$  of the full order snapshots, for each parameter in the training set  $\mathcal{S} = \{\mu_1, \dots, \mu_p\}$ . Note that this procedure is the same which we presented in section 2.3.1. However, at this point we do not build the matrix  $\mathcal{X}_2$ : instead we perform  $p$  separate DMDs, one for each matrix  $\tilde{\mathbf{X}}^{\mu_i}, i \in \{1, \dots, p\}$ . Namely, for each  $\mu_i$  with  $i \in \{1, \dots, p\}$  we consider the matrices  $\tilde{\mathbf{X}}_1^{\mu_i}, \tilde{\mathbf{X}}_2^{\mu_i} \in \mathbb{R}^{n \times (N-1)}$  which results from taking  $N - 1$  columns of  $\tilde{\mathbf{X}}^{\mu_i}$  — as in the standard DMD method — and we approximate the DMD operator  $\tilde{\mathbf{A}}^{\mu_i} \in \mathbb{R}^{n \times n}$  such that  $\tilde{\mathbf{X}}_2^{\mu_i} = \tilde{\mathbf{A}}^{\mu_i} \tilde{\mathbf{X}}_1^{\mu_i}$ . After that the prediction of future POD coefficients is carried out independently for each tested parameter using eq. (2.8).

According to our experiments this approach is more reliable than that presented in section 2.3.1 when applied on systems for which the variation of the parameter leads to a considerable change in the behavior. Different instances of these systems (i.e. realizations with different parameters) are often weakly coupled, in the sense that it is usually hard to find recurrent patterns, if not possible at all. The application of the method presented in this section partially fixes the problem.

## 2.4 Online phase

Using the features presented in section 2.1 and the methods proposed in section 2.3.1 and section 2.3.2 we are able to exploit eq. (2.4) to predict the value of POD coefficients in future time instants. To simplify the discussion we are going to assume that the approach is used to predict

---

**Algorithm 2** Dynamic Mode Decomposition for parametric problems — Partitioned

---

**Input:**  $\mathbf{X}^{\mu_1}, \dots, \mathbf{X}^{\mu_p} \in \mathbb{R}^{m \times N}$

Construct the matrix  $\mathcal{X}_1 \in \mathbb{R}^{m \times Np}$   
Compute the POD coefficients of the columns of  $\mathcal{X}_1$   
Store the coefficients into  $\tilde{\mathbf{X}}^{\mu_i}, i \in \{1, \dots, p\}$   
Compute  $\tilde{\mathbf{x}}_{N+1}^{\mu_i}$  using eq. (2.4) on  $\tilde{\mathbf{X}}^{\mu_i}, i \in \{1, \dots, p\}$ .  
**for**  $i \in \{1, \dots, p\}$  **do**  
    Compute the DMD operator  $\tilde{\mathbf{A}}^{\mu_i}$  by fitting  $\tilde{\mathbf{X}}^{\mu_i}$   
**end for**

---

just one time instant, namely  $t_*$ . It will be clear that this discussion can be easily extended to a more general case.

After the *offline phase* we can exploit the DMD operator (or the several DMD operators in case of the partitioned approach) to predict the reduced snapshots at time  $t_*$  for the parameters in the training set  $\mathcal{S} = \{\mu_1, \dots, \mu_p\}$ , obtaining then the matrix  $\mathcal{X}_3$  which has the following form:

$$\mathcal{X}_3 = \begin{bmatrix} | & \dots & | \\ \tilde{\mathbf{x}}_{N+1}^{\mu_1} & \dots & \tilde{\mathbf{x}}_{N+1}^{\mu_p} \\ | & \dots & | \end{bmatrix} \in \mathbb{R}^{n \times p} \quad (2.9)$$

The matrix  $\mathcal{X}_3$  has one row for each retained POD coefficient and one column for each realization of the parametric system used to train the algorithm.

In the *online phase* we explore the *solution manifold* for untested parameters in  $\mathbb{P}$  using an approach similar to POD with Interpolation (PODI) [1, 3]. This means that the mapping between the parameter space and the POD space is approximated by using some regression or interpolation techniques. Formally we train the regressor  $\mathcal{I} : \mathbb{P} \rightarrow \mathbb{R}^n$  on the system of  $p = |\mathcal{S}|$  vectorial equations  $\mathcal{I}(\mu_i) = \tilde{\mathbf{x}}_{t_*}^{\mu_i}$  for  $i \in \{1, \dots, p\}$ . Using  $\mathcal{I}$  we are able to approximate a new reduced snapshot  $\tilde{\mathbf{x}}_{t_*}^{\mu_*}$  for an untested parameter  $\mu_*$ . We remark that in order to obtain the approximated reduced snapshot we need a multidimensional regressor; alternatively a single regressor can be built for any components of the reduced snapshots.

At this point we are able to recover the approximated full order vector  $\mathbf{x}_{t_*}^{\mu_*} \approx \hat{\mathbf{x}}_{t_*}^{\mu_*} = \mathbf{U}_n \tilde{\mathbf{x}}_{t_*}^{\mu_*} \in \mathbb{R}^m$ , which is the predicted realization of the system with the untested parameter  $\mu_*$  in the future time instant  $t_*$ .

---

**Algorithm 3** Dynamic Mode Decomposition for parametric problems — Online phase

---

**Input:** The operator  $\tilde{\mathbf{A}}$  (or the operators  $\{\tilde{\mathbf{A}}^{\mu_i}\}_{i=1}^p$ )

**Input:** the POD basis  $\mathbf{U}_n$

**Input:** the parameter  $\mu_* \in \mathbb{P}$

**Input:** the time instant  $t_*$

Predict the reduced snapshots  $\tilde{\mathbf{x}}_{t_*}^{\mu_i} \in \mathbb{R}^n$  using DMD operator(s) for  $i \in \{1, \dots, p\}$   
Build the mapping  $\mathcal{I} : \mathbb{P} \rightarrow \mathbb{R}^n$  such that  $\mathcal{I}(\mu_i) = \tilde{\mathbf{x}}_{t_*}^{\mu_i}$  for  $i \in \{1, \dots, p\}$   
Approximate the new reduced snapshot  $\tilde{\mathbf{x}}_{t_*}^{\mu_*} = \mathcal{I}(\mu_*)$   
Recover the full dimensional representation  $\hat{\mathbf{x}}_{t_*}^{\mu_*} = \mathbf{U}_n \tilde{\mathbf{x}}_{t_*}^{\mu_*} \in \mathbb{R}^m$

---

## 2.5 DMD stabilization

It may happen in some cases that DMD produces *divergent* modes, which means that the eigenvalues associated with these modes reside outside the unit circle (*modulo* greater than one). This is a very problematic aspect if we intend to perform prediction on future time instants, since these eigenvalues are very likely to diverge due to Eq. (2.4), making the prediction unusable. Such behaviour is strictly correlated to the problem in hand, but it is also affected by numerical approximation, noisy data or a limited set of input snapshots, which may induce the DMD to compute divergent modes even when applied to stable systems.

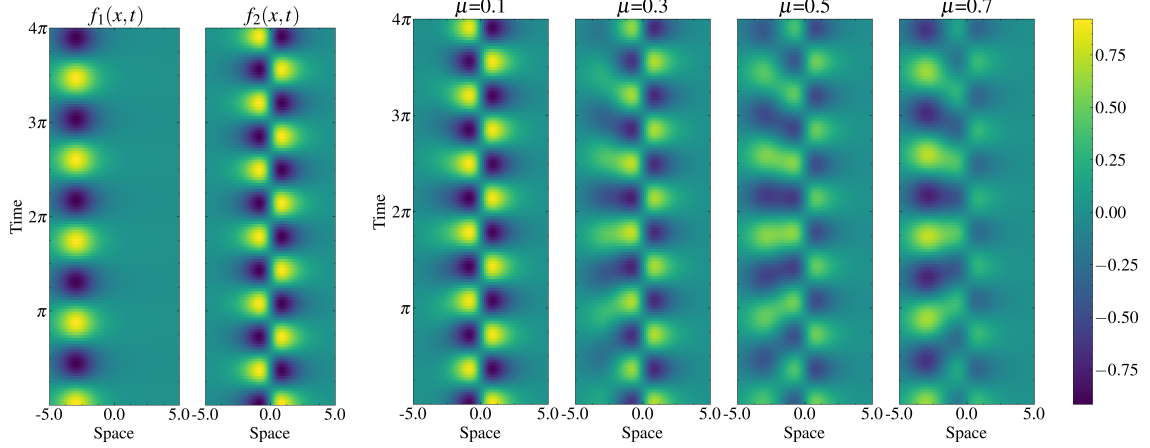


Figure 1: On the left, the two simple functions which we are using for the composition. We consider 10 values of  $\mu$  to train our algorithm, the realizations corresponding to  $\mu \in \{0.1, 0.3, 0.5, 0.7\}$  are shown on the right.

To overcome these difficulties, we propose here a simple approach to stabilize the DMD operator by looking at its eigenvalues. The main idea is to keep only the stable modes, discarding all the diverging and converging eigenvectors, then employing the Eq. (2.4) using the selected eigenpairs. We consider a threshold  $\epsilon$  for the selection. First of all, we discard all the DMD modes that have the modulo of the corresponding eigenvalue greater than  $1 + \epsilon$ , which we remark be the divergent ones. We perform the same procedure also to convergent modes — which tends to have a nil contribution advancing in time —, removing the modes that have the corresponding eigenvalue inside the unit circle. Finally, the eigenvalues of the remaining modes are projected onto the unity circle (i.e. the eigenvalue is normalized), in order to stabilize the operator. Formally, we manipulate the eigenvalues such that:

$$\lambda_i^{\text{stable}} = \begin{cases} 0 & \text{if } |\lambda_i - 1| > \epsilon \\ \frac{\lambda_i}{|\lambda_i|} & \text{otherwise} \end{cases} \quad \text{for } i = 1, \dots, r. \quad (2.10)$$

Defining  $\mathbf{\Lambda} = \text{diag}(\lambda_1^{\text{stable}}, \dots, \lambda_r^{\text{stable}})$  is sufficient to obtain the stabilized version of operator.

### 3 Numerical results

In this section we present the numerical results obtained using the two approaches discussed in sections 2.3.1 and 2.3.2 on three problems in different topics.

#### 3.1 Numerical study 1: System of algebraic equations with linear parameter dependency

For our first experiment we consider the simple system depicted in fig. 1, which is the parametrized composition of two time dependent functions:

$$f(x, t, \mu) = \mu f_1(x, t) + (1 - \mu) f_2(x, t), \quad \begin{cases} f_1(x, t) = \text{sech}(x + 3) \exp(i2.3t) \\ f_2(x, t) = 2 \text{sech}(x) \tanh(x) \exp(i2.8t) \end{cases} \quad (3.1)$$

We consider the time instants set  $\mathcal{T}$  to be an equispaced sampling of the time frame  $[0, 4\pi]$  (we retain  $N = 129$  samples); the spatial domain  $\Omega$  is  $[-5, 5]$  (we take  $m = 1000$  equispaced samples from this interval). Therefore our output function, which is a discrete version of that shown in eq. (3.1), has the form  $\mathbf{f}_k^\mu \in \mathbb{R}^{1000}, k \in \mathcal{T}$ : each component of the vector corresponds to one of the 1000 samples of the space domain  $\Omega$ . From the formulation of the problem it is clear that the dependency of the system on the parameter  $\mu$  is linear. We consider the training parameters set  $\mathcal{S}$  to be an equispaced sampling of the set  $[0, 0.9]$  (we retain  $p = 10$  samples from this interval).

Considering the linear dependency of the system on the parameter  $\mu$ , we apply the monolithic method discussed in section 2.3.1. From fig. 2a we infer that the optimal value for  $n$  (the number

of POD modes retained for each realization of the system) is  $n = 2$ . The optimality of this value is also confirmed by the fact that the corresponding POD modes (fig. 2b) are physically coherent with the system depicted in fig. 1. After the application of DMD (we take only the first two modes employing the singular values criteria, fig. 3a) we obtain the matrix  $\Phi \in \mathbb{R}^{np \times 2} = \mathbb{R}^{20 \times 2}$  of the two DMD modes extracted from  $\mathcal{X}_2$  defined like in eq. (2.7). In order to visualize the results of the analysis we split  $\Phi$  in  $p$  sub-components  $\Phi_i \in \mathbb{R}^{n \times 2} = \mathbb{R}^{2 \times 2}$ : each column contain the part of the DMD mode relative to a particular parameter. After that we use the matrix of POD modes to recover the full-dimension appearance of each DMD mode (fig. 3b). The dynamics of the two DMD modes are then visualized in fig. 3c, as expected they are periodic functions.

We are now able to start the *online phase*: using DMD modes and dynamics we approximate POD coefficients corresponding to future time instants ( $t > N$ ) for tested values of the parameter. We would like to double the amplitude of the time frame, namely we intend to approximate the behavior of the system until  $t = 8\pi$  (we keep the same time difference between consecutive snapshots). We also consider three untested parameters:  $\mu_x \in \{0.375, 0.525, 0.875\}$ . After the examination of fig. 4a we can assume that POD coefficients are arranged roughly along a straight line for all time instants. This situation is ideal for the interpolation, assuming that DMD preserves this kind of arrangement. In fig. 4b we plot the results of the interpolation, versus the expected POD coefficients, which we obtained projecting the matrix  $\mathbf{X}^{\mu_x}$  onto the reduced POD subspace spanned by the columns of the matrix  $\mathbf{U}_n$  of POD modes, where  $\mu_x$  is any of the untested parameters which we mentioned above.

In fig. 5 we depict the system predicted/interpolated using our approach, for the three untested parameters  $\mu_x \in \{0.375, 0.525, 0.875\}$ , in the doubled time frame  $[0, 8\pi]$ . The non-null error is most likely given by the fact that we considered a small number of POD modes with respect to the high dimensionality of the original system.

### 3.2 Numerical study 2: An heat conductivity problem

We consider now a parametric nonlinear unsteady heat problem introduced in [5, 9]. We want to compute the unknown  $u(\mathbf{x}, t, \boldsymbol{\mu})$  with  $\mathbf{x} = (x_1, x_2) \in \Omega = [0, 1] \times [0, 1]$ ,  $t \in [0, 2]$  and  $\boldsymbol{\mu} = (\mu_1, \mu_2) \in \mathbb{P} = [0.01, 10]^2$  such that

$$\begin{cases} \frac{\partial u}{\partial t} - \nabla^2 u = 100 \sin(2\pi x_1) \sin(2\pi x_2) \sin(2\pi t) - \frac{\mu_1}{\mu_2} (e^{\mu_2 u} - 1) & \text{in } \Omega, \\ u = 0 & \text{on } \partial\Omega. \end{cases} \quad (3.2)$$

The discrete solution of such a problem is obtained by employing the finite element framework. The 2D spatial domain is divided in 800 triangular cells with P1 element.

We consider 95 instances of the system. The distribution of the parameters (tested and untested) is depicted in fig. 6a, alongside the physical appearance of the system at several (known)

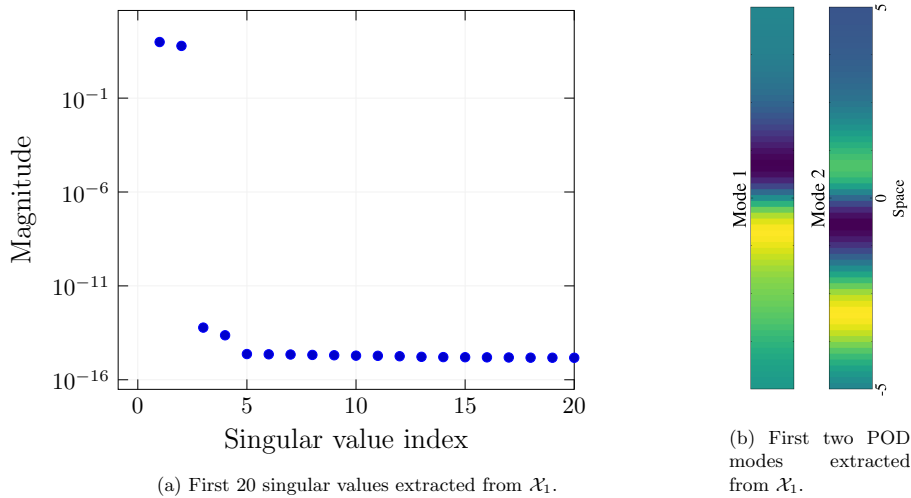


Figure 2: Looking at singular values of the system, on the left, we deduce that the most contribution is given by the first two POD modes. We drew those modes on the right.

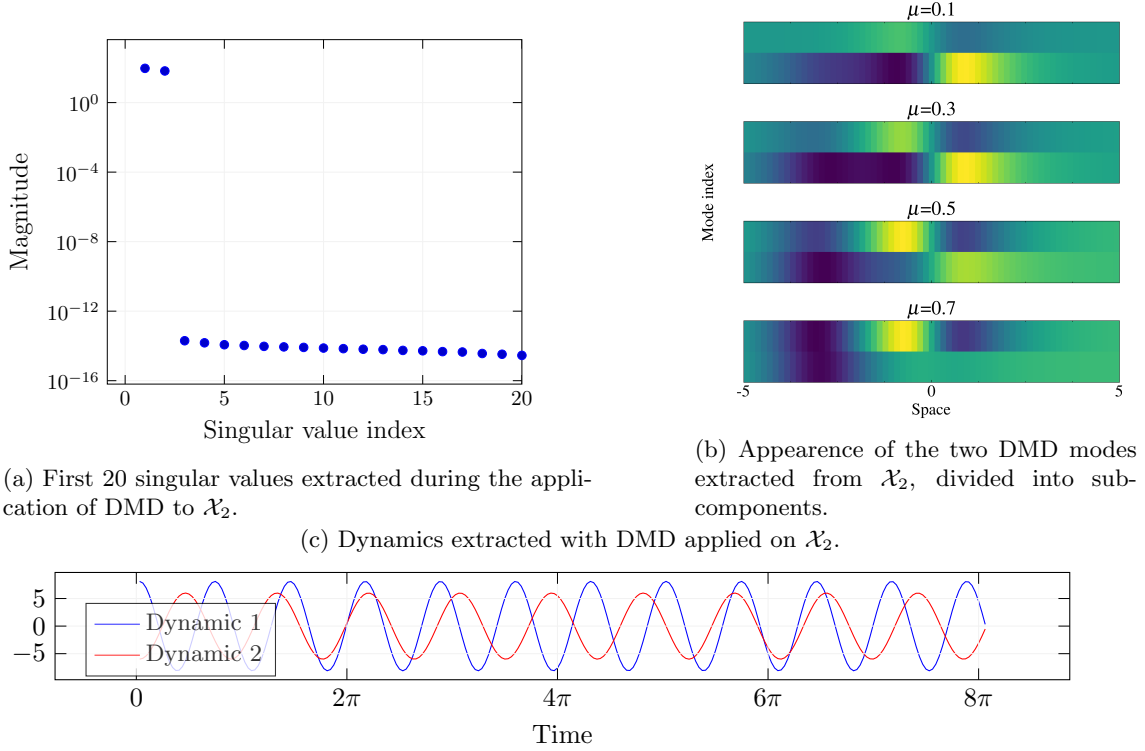
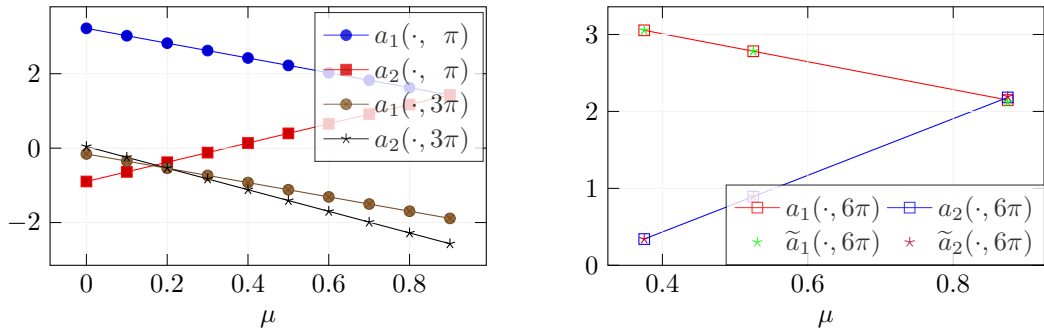


Figure 3: Results of the application of DMD to the matrix  $\mathcal{X}_2$ : singular values (fig. 3a), DMD modes (fig. 3b), dynamics of the extracted modes (fig. 3c).

time instants. For all the parametric samples, we collect 86 snapshots equispaced in the time window  $[0, 85]$ . We retained 30 POD modes for the reduced space, and did not perform an additional reduction during the DMD-step. We attempt to predict/interpolate the system for three more *untested* parameters, depicted in red ( $\circ$ ) in fig. 6a, which we collect into the set  $\mathcal{Q}$ . We also consider an extended time frame  $86 \leq t \leq 100$ .

In fig. 7a we observe that, unlike the system considered for the first experiment, POD applied on  $\mathcal{X}_1$  needs a considerable number of POD modes in order to capture all the significant characteristic structures of the parametric system. The first hard step occurs around the 100-th singular value, however we preferred to choose a lower threshold in order to keep the interpolation error under control. We can still see that the first modes are the most significant ones, even when POD is applied simultaneously on more realizations of the same parametric system.

In fig. 8 we see that the distribution of POD modal coefficients (starting from the second one) is



(a) First and second POD coefficients for *tested* parameters at several time instants.

(b) Interpolated/predicted and expected POD coefficients at  $t = 6\pi$ .

Figure 4: On the left we show the arrangement of POD coefficients for  $t = \pi, 3\pi < N$  as  $\mu$  varies. On the right, the results of the prediction and interpolation of five untested parameters for  $t = 6\pi > N$ .

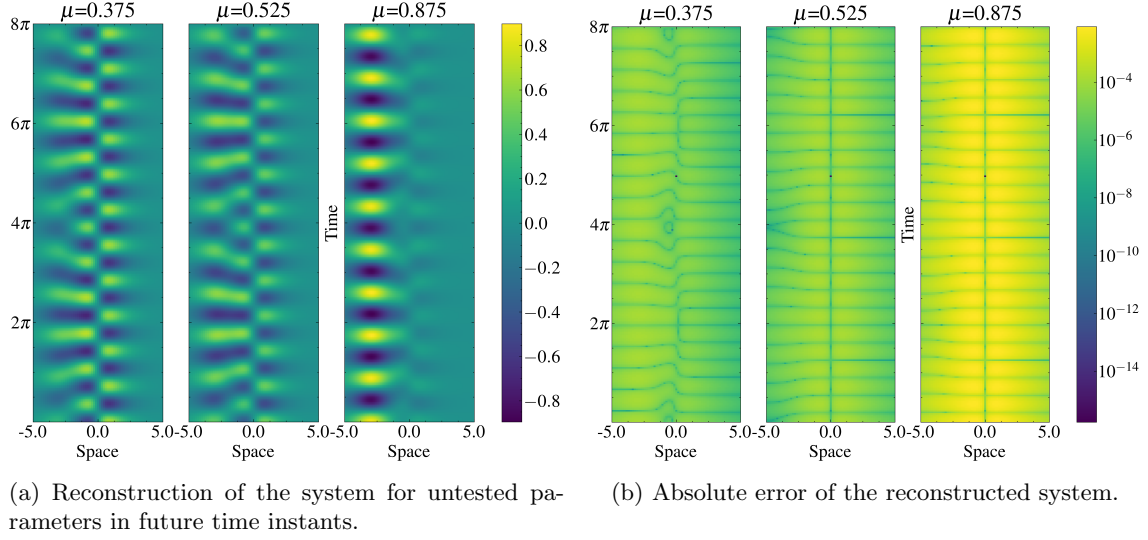


Figure 5: On the left we plot the result of the algorithm discussed in section 2.3.1; on the right we show the absolute error between the expected and reconstructed system.

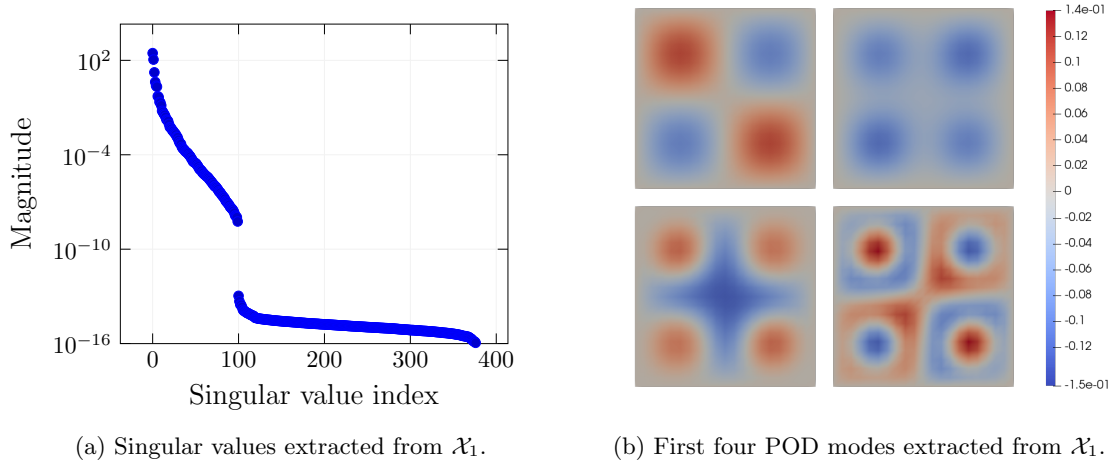
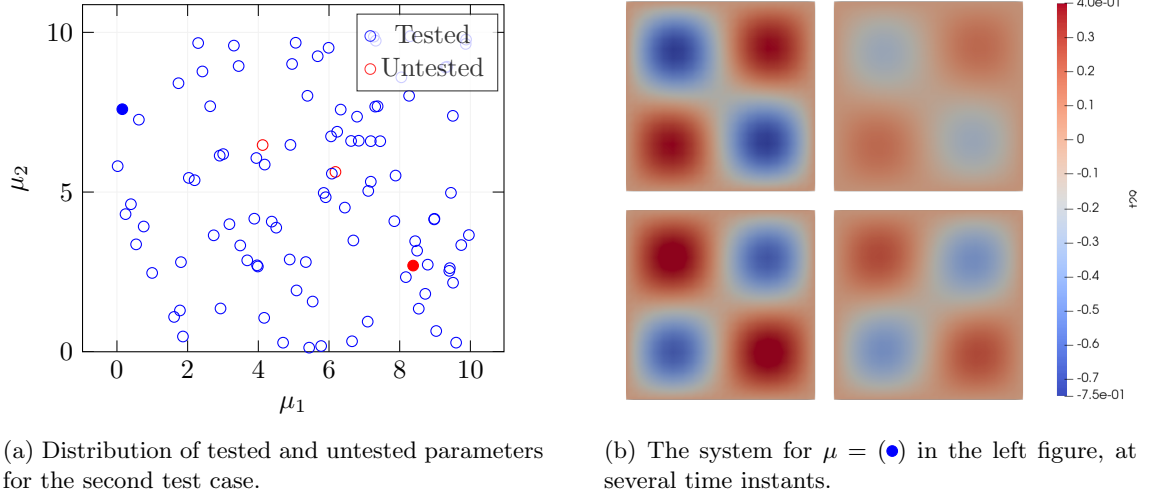
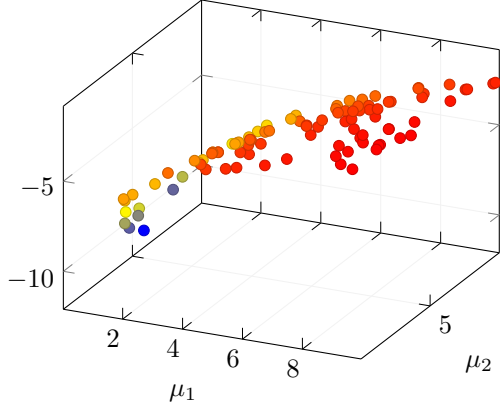
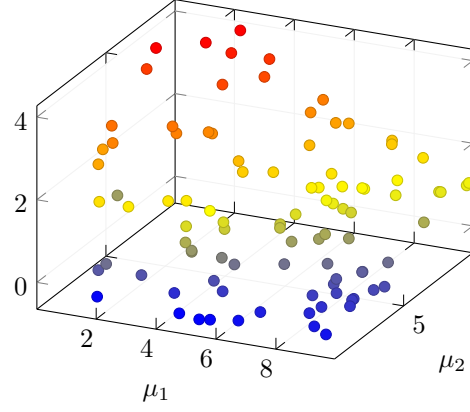


Figure 7: Unlike the system shown in section 3.1, it is clear that we would need to consider an higher number of POD modes in this case in order to guarantee an high fidelity reconstruction.



(a) First POD coefficient at  $t = 10$ .



(b) Second POD coefficient at  $t = 10$ .

Figure 8: The first POD coefficients (fig. 8a) for each value of  $\mu$  are arranged roughly on a flat surface. However, the second POD coefficients (fig. 8b) are much more scattered, but we could attempt the interpolation using a linear interpolator, or the algorithm K-NearestNeighbors.

less regular than the distribution in the first experiment.

In fig. 9 we plot the result of the interpolation (we used a linear interpolator) for two *tested* and three *untested* parameters. The error on POD coefficients for tested parameters are visualized to check in which step we introduce the biggest error. In fact we can see that in the unknown time frame (starting from  $t = 85$ ) the error on tested POD coefficients starts to increase slightly, while the error on untested POD coefficients remains stable. This means that the error introduced with the prediction provided by DMD is negligible with respect to the error introduced by interpolators.

Finally, we plot the prediction for one of the *untested* parameters and unknown time instants computed using our approach, alongside the truth solution, the relative and absolute error. The red cross at the center of fig. 11b is given by the fact that that region of  $\Omega$  maintains values around zero for the majority of time instants, therefore the relative error appears high with respect to the neighborhoods. The same “problem” does not appear in fig. 11a, since no division is performed.

For this problem we consider a set of experiments aimed at checking the sensitivity of the approach on the number of tested parameters and on the size of the time frame used during the training of DMD. We also take into account several interpolators with different features for the online phase, in order to assess which one could vally provide better performances. In order to visualize such measurements we are going to compute a scalar function  $e_{\mathcal{I}}(\mathcal{S}, \mathcal{T}, t, \mu)$  defined as the relative error at time  $t$  between the reconstructions of the system in the untested parameter  $\mu \in \mathcal{Q}$

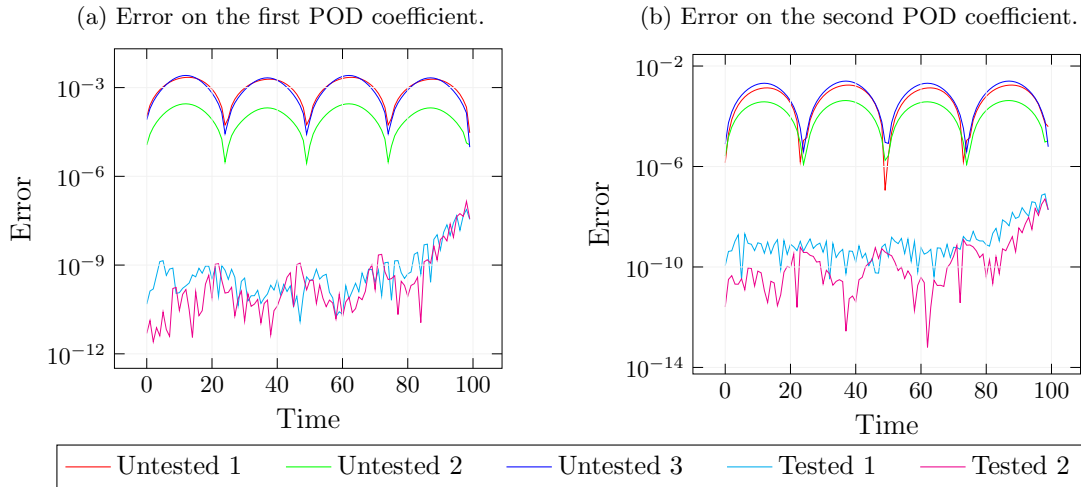
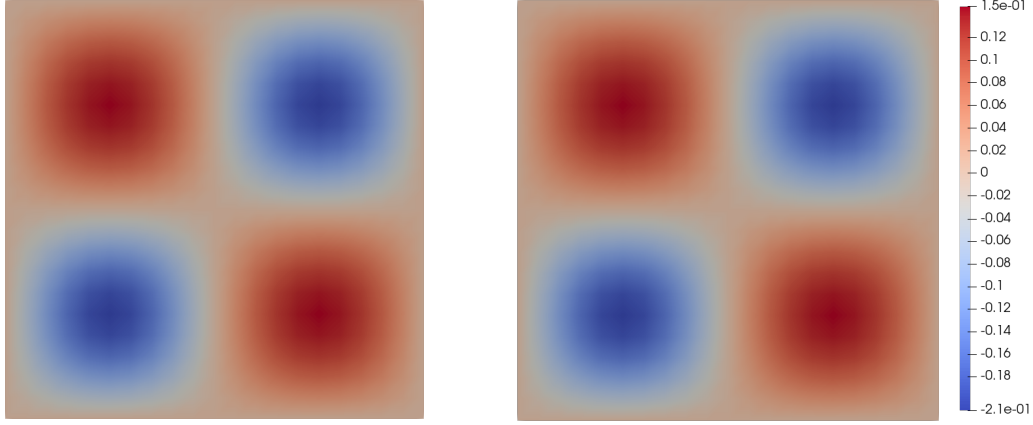
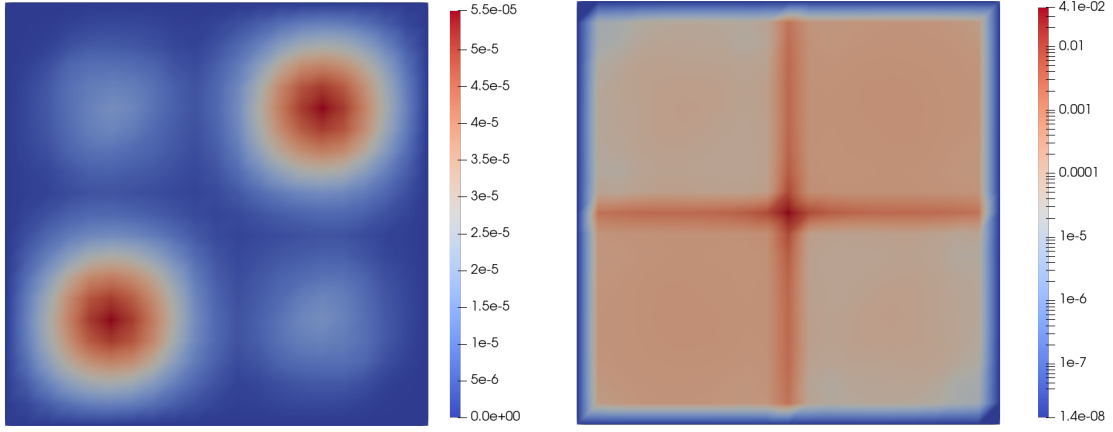


Figure 9: Evolution over time of the absolute error on the first and second POD coefficient for several *tested* and *untested* values of the parameter.



(a) Original system.

(b) Output returned by pDMD.



(a) Absolute error.

(b) Relative error.

Figure 11: Result for the untested parameter represented by (•) in Figure 6a, at  $t = 91$ .

and the high-fidelity validations. Since we consider more than one  $\mu$  for this measurement (we recall that  $\mathcal{Q}$  is a set of untested parameters which we presented above), we are going to consider the mean relative error. Formally we define it as:

$$e_{\mathcal{I}}(\mathcal{S}, \mathcal{T}, t) = \frac{1}{|\mathcal{Q}|} \sum_{\mu \in \mathcal{Q}} \frac{\|\hat{\mathbf{x}}_t^{\mu}[\mathcal{S}, \mathcal{T}] - \mathbf{x}_t^{\mu}\|_2}{\|\mathbf{x}_t^{\mu}\|_2} \quad (3.3)$$

where  $\hat{\mathbf{x}}_t^{\mu}[\mathcal{S}, \mathcal{T}]$  refers to the snapshots approximation of the algorithm trained over  $\mathcal{S}$  parametric samples and  $\mathcal{T}$  time instants. We would like to investigate the accuracy of the prediction in the experiments, therefore we are going to evaluate the value of  $e_{\mathcal{I}}(\mathcal{S}, \mathcal{T}, t)$  for several combinations of the parameters taken into account, in order to assess the sensitivity of the proposed method on the different factors which affect the quality of the reconstruction.

Since we need to interpolate values on a 2-dimensional surface, during the experiment we are going to consider the following regressors, for which we provide a brief explanation:

- *Linear*: divides the surface in 2-dimensional simplices, and interpolates linearly on each sub-surface [10];
- *Cubic*: return the value determined from a piecewise cubic polynomial surface [10];
- *Nearest neighbor*: Return the nearest value in the dataset [2];
- *GPR*: Interpolates using a Gaussian Process [22].

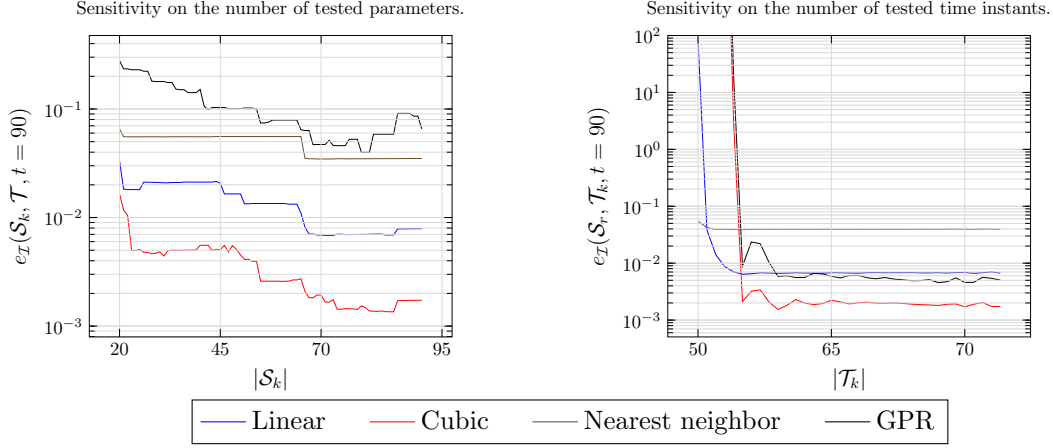


Figure 12

In the first experiment we consider a random initial training set  $\mathcal{S}_0$  which contains 20 parameters. We add random parameters one by one in such a way that  $\mathcal{S}_{k+1} = \mathcal{S}_k \cup \text{rand}(\mathbb{P} - \mathcal{S}_k)$ , where the function `rand` extracts a random member from the set passed as argument, and  $\mathbb{P}$  is the set which contains all the allowed parameters for the parametric system taken into account. This procedure is iterated  $r$  times, until the size of the training set (which we refer to as  $p = |\mathcal{S}_r|$ ) is equal to 95. In this experiment the size of the time frame used for the training phase is fixed ( $\mathcal{T} = \{t \mid 1 \leq t \leq 85\}$ ). We also consider five distinct untested parameters  $\hat{\mathcal{S}}$  extracted randomly from the set  $\mathbb{P} - \mathcal{S}_r$ . The distribution of parameters used for the training phase and those used to validate the approach is plotted in fig. 6a.

Using the approach presented in section 2.3.2, for each training set  $\mathcal{S}_k$  we interpolate the system in the untested parameters  $\hat{U}$  and predict the system in the time frame  $86 \leq t \leq 100$ . We also evaluate the function  $e_I(\mathcal{S}_k, \mathcal{T}, t)$  for each possible combination of its arguments (keeping  $\mathcal{T}$  fixed, and  $k \in \{0, \dots, r\}$ ). The value  $e_I(\mathcal{S}_k, \mathcal{T}, t=90)$  is shown in the left part of fig. 12: we depict the dependency of the mean relative error on the cardinality of the set  $\mathcal{S}_k$  of training time instants considered during the offline phase. It is clear that the error decreases in general when the number of tested parameter increases as expected; however there is a little bit of *overfitting* around  $p = 90$  for all the interpolators.

In the second experiment the set of tested parameters is fixed ( $p = 95$ , we consider the biggest training set  $\mathcal{S}_r$  from the last experiment). We consider an initial time frame  $\mathcal{T}_0$  which spans from 1 to 50; at each step we add one time instant to the training time frame in such a way that  $\mathcal{T}_{k+1} = \min(\mathbb{N} - \mathcal{T}_k)$ . We iterate this process  $q$  times, until  $85 \in \mathcal{T}_r$ .

Then we execute the same operations performed in the last experiment: we interpolate and predict the system in the time frame  $86 \leq t \leq 100$  for five untested parameter (the same of the last experiment), and we compute the values of the function  $e_I(\mathcal{S}_r, \mathcal{T}_k, t)$  for all the possible combinations of its parameters (this time we keep  $\mathcal{S}_r$  fixed and let  $k \in \{0, \dots, q\}$ ).

The results of the experiment are plotted in the right part of fig. 12 for  $t = 90$ , where we depict the dependency of the error function on the cardinality of the set  $\mathcal{T}_k$  of training time instants considered during the offline phase. After a critical phase, which is most likely due to the internal working of DMD (we remark that the error taken into account is relative), the error decodes as the number of time instants increases, which is the expected behavior; finally (time frame  $0 \leq t \leq 60$ , approximately) the error becomes almost stable.

### 3.3 Numerical study 3: Navier-Stokes's cylinder

The third numerical experiment is the simulation of a parametric Navier-Stokes flow passing around a circular cylinder. The equations that describes the problem are:

$$\begin{cases} \frac{\partial u}{\partial t} + (u \cdot \nabla)u + \nabla p - \nu \Delta u = f & \text{on } \Omega \times [0, T], \\ \nabla \cdot u = 0 & \text{on } \Omega \times [0, T], \\ u_x = \mu & \text{in } \Gamma_{\text{IN}} \times [0, T], \\ u = 0 & \text{in } \Gamma_{\text{CYL}} \cup \Gamma_{\text{S}} \cup \Gamma_{\text{N}} \times [0, T], \end{cases} \quad (3.4)$$

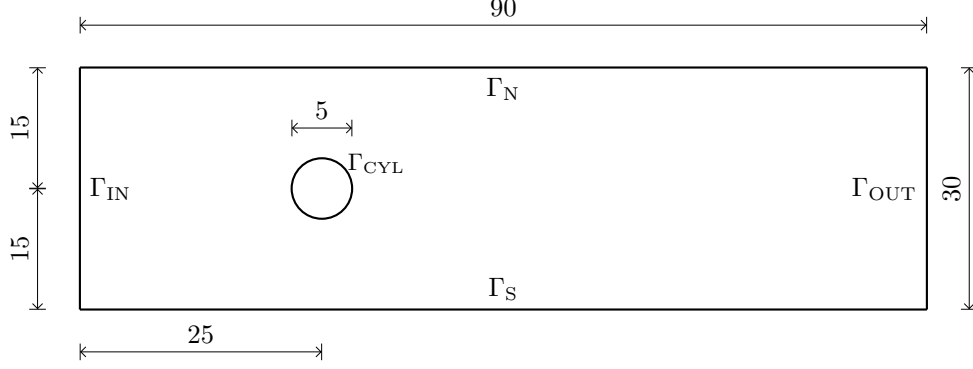


Figure 13: The domain  $\Omega$  for the parametric Stokes flow simulation.

where  $\Omega$  is the 2-dimensional rectangular domain containing a circular hole (which represents the cylinder), depicted in Figure 13. We set  $T = 5000$  and  $\Delta t = 0.2$  for time discretization in the full-order model. The parameter  $\mu$  controls the horizontal component of the velocity of the fluid entering the inlet (the vertical component is set to zero), and consequently also the Reynolds number. Since the parameter space is set to  $\mathbb{P} = [0.0001, 0.002]$ , we are here in laminar regime, making unnecessary the employment of turbulence models. We impose on the physical walls (namely the cylinder and the two horizontal walls) the no-slip boundary condition. For the training set, we considered 14 equispaced values of  $\mu \in \mathbb{P}$  and 200 time instants in the time window  $[4000, 4800]$  with  $\Delta t = 4$ . Initial time steps show the propagation of boundary condition, obfuscating the real physical phenomena, and then they are discarded by the training set.

We employed the *partitioned* procedure discussed in section 2.3.2 to test the results of our approach on the two untested parameters  $\mu = 0.0005$ ,  $\mu = 0.001775$ , for which we predicted an approximated solution for the time instants between 4800 and 5000. For this experiment we only considered the horizontal component of the point-wise velocity of the fluid, in order to simplify the presentation of the results.

We considered 40 POD modes, and did not perform an additional reduction during the application of DMD. We used HODMD, the variant of DMD described in section 2.2, since the spatial complexity (which is 40 in this case, since we only retain 40 POD coefficients) was much lower than the number of time instants considered for the training (we remind to the reader that for the modular approach DMD is applied individually to each matrix  $\mathbf{A}_{\mu_i} \in \mathbb{R}^{n \times N}$  of POD coefficients). We also used the stabilization approach presented in section 2.5 and retained only DMD modes corresponding to eigenvalues whose distance from the unit circle was at most  $\epsilon = 10^{-3}$ . As we can see in fig. 16, thanks to such approach we are able to discard all the divergent modes, obtaining a good prediction also in test time window  $[4800, 5000]$  (relative mean error equal to 0.04). We remark that without stabilization the error for future time instants is several order of magnitude bigger, since the exponential growth of some modes.

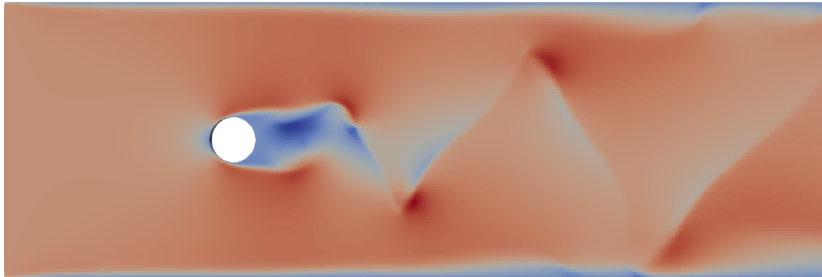


Figure 14: The system for  $\mu = 0.0015$  (one of the tested parameters) at  $t = 850$ .

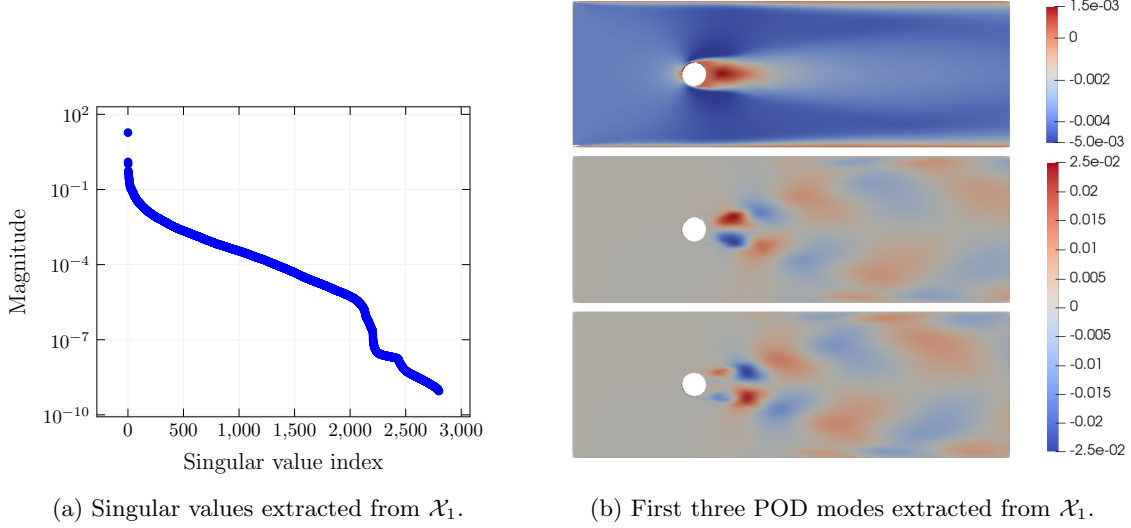


Figure 15

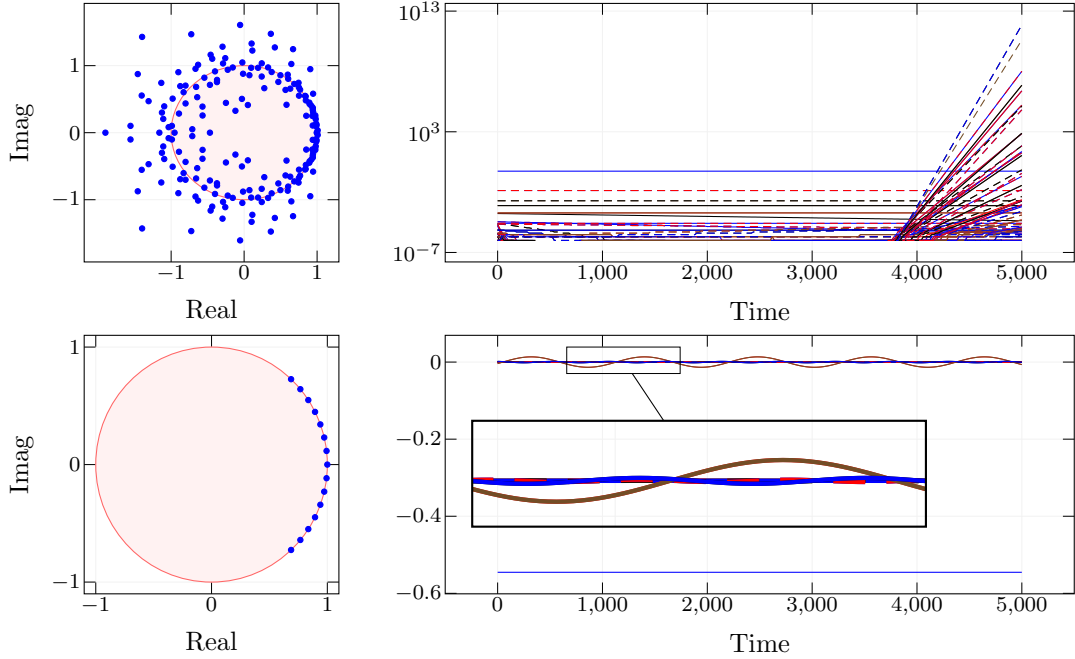


Figure 16: DMD Stabilization in the Navier-Stokes problem. On top, DMD eigenvalues and dynamics before stabilization. On bottom, DMD eigenvalues and dynamics after stabilization.

In section 3.3 we show the physical appearance of the system for one of the tested parameters. After the examination of the decay of the singular values of the matrix  $\mathcal{X}_1$  (fig. 15a) we observe that the system is poorly represented if we use a low number of POD modes. However, the proposed approach relies on the interpolation of POD modal coefficients, which becomes less and less precise (for same number of samples) at higher dimensions. Therefore we expect an increase in the error if the number of POD modes is increased. While we see some advantages in raising the number of POD modes (especially for systems like this one) it is recommended to look for a compromise between the error given by regression and error given by POD space projection.

In fig. 15b we observe the first POD modes, which are the characteristic modes for low values of the parameter (first mode, in this case the system is stationary and has almost no waves) and high values of the parameter (second and third modes). This confirms that POD is able to extract dominant structures simultaneously from different instances of a parameterized system.

In fig. 17 we provide an analysis of the error on the first POD coefficients as a function of

the time, in the predicted time frame ( $4800 \leq t \leq 5000$ ). Like in the previous cases, the error is computed with a multiplication between the high-dimensional matrix which represents the system in the untested parameters and the matrix  $\mathbf{U}_r$  of POD modes obtained during the *offline phase*. Again, POD coefficients do not appear to be placed along a linear path as  $\mu$  varies, however we are able to obtain an acceptable approximation for intermediate values of the parameter.

Finally, in figs. 18 and 19 we show the results of the proposed algorithm (above) against the truth solution (below). In the regions outside the cylinder trail the pointwise error is higher, due to the low number of POD modes we considered. However we are able to obtain an acceptable approximation of the region of  $\Omega$  in the trail: we obtain a low pointwise error near the cylinder; as we procede towards the right wall the error increases, but we are able to capture and represent the characteristic behaviors of the waves.

## 4 Conclusions

In this contribution we introduced a novel approach to exploit dynamic mode decomposition even in case of parametrized dynamical systems. Keeping the data-driven nature and the offline-online subdivision of the original algorithm, we exploit reduction and regression techniques in order to obtain a quick approximation of the output of interest for new untested parameters, in any temporal instant. Such methodology demonstrated its effectiveness with three different numerical experiments, presenting some limitations where the original model is not well represented in a POD space, as for the Navier-Stokes problem.

A possible improvement of the method proposed in this work can be a smarter strategy to group the modal coefficient in the *partitioned* approach. In this work we presented the results obtained by grouping them according to the parameter, but the accuracy can be improved by some classification techniques, such as clustering. The goal is to put into the same cluster parameters which lead to similar realizations of the dynamical system, according to some notion of similarity. For instance, we may group parameters which are close to each other according to some norm defined on  $\mathcal{P}$ . This modification may fix some of the problems which made us conceive the partitioned approach as opposed to the monolithic one, while keeping the benefits of the latter. It may be interesting to consider intersecting clusters, in order to improve the linking between different groups of parameters. Another further improvement of the proposed framework could be the usage of other dimensionality reduction techniques in order to replace the POD method.

## Acknowledgements

This work was partially supported by European Union Funding for Research and Innovation — Horizon 2020 Program — in the framework of European Research Council Executive Agency: H2020 ERC CoG 2015 AROMA-CFD project 681447 “Advanced Reduced Order Methods with Applications in Computational Fluid Dynamics” P.I. Gianluigi Rozza.

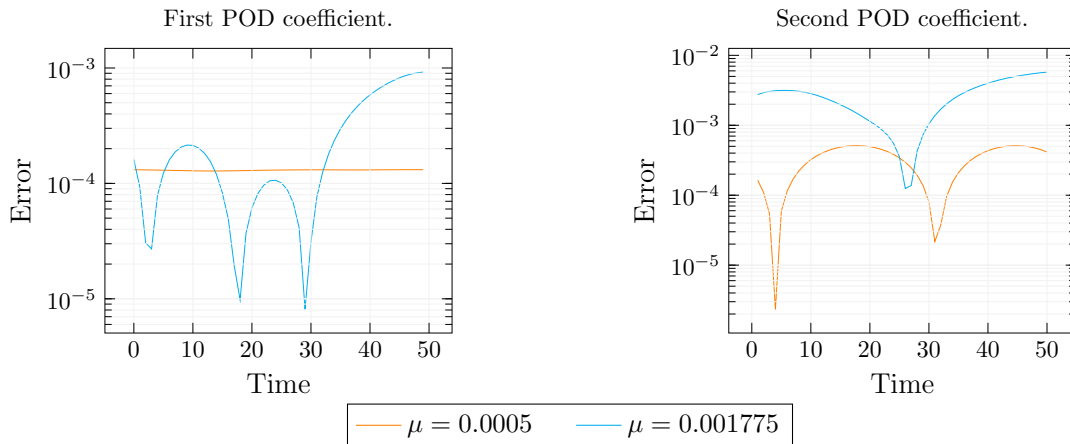


Figure 17: Absolute error for the first (on the left) and second (on the right) POD coefficients.

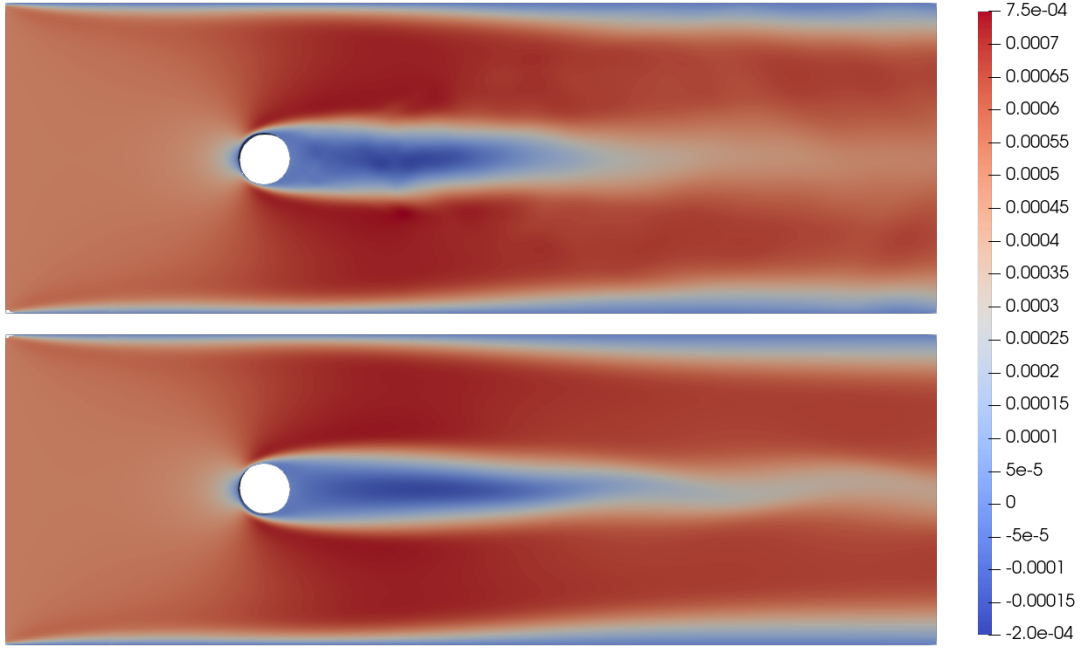


Figure 18: Results of the proposed algorithm (above) for the Cylinder problem for  $\mu = 0.0005$  at  $t = 1250$  (truth solution below).

## References

- [1] D. Amsallem and C. Farhat. Interpolation method for adapting reduced-order models and application to aeroelasticity. *AIAA journal*, 46(7):1803–1813, 2008.
- [2] N. Bhatia et al. Survey of nearest neighbor techniques. *arXiv preprint arXiv:1007.0085*, 2010.
- [3] N. Demo, M. Tezzele, G. Gustin, G. Lavini, and G. Rozza. Shape optimization by means of proper orthogonal decomposition and dynamic mode decomposition. submitted. *arXiv*

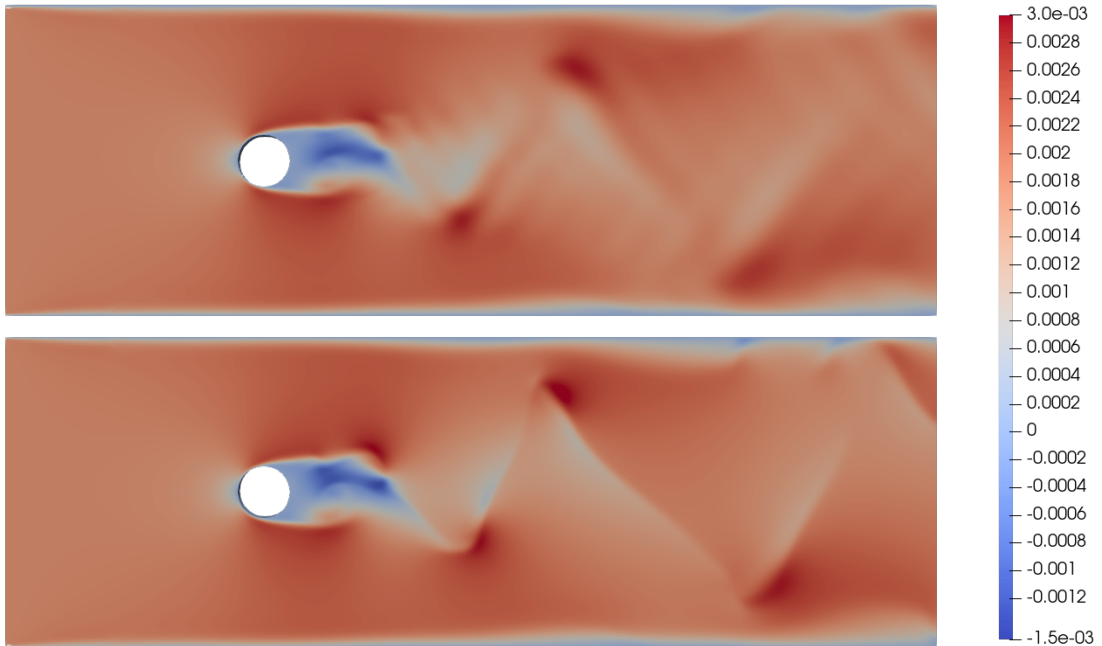


Figure 19: Results of the proposed algorithm (above) for the Cylinder problem for  $\mu = 0.001775$  at  $t = 5000$  (truth solution below).

preprint *arXiv:1803.07368*, 2018.

- [4] S. Georgaka, G. Stabile, G. Rozza, and M. J. Bluck. Parametric pod-galerkin model order reduction for unsteady-state heat transfer problems. *arXiv preprint arXiv:1808.05175*, 2018.
- [5] M. A. Grepl, Y. Maday, N. C. Nguyen, and A. T. Patera. Efficient reduced-basis treatment of nonaffine and nonlinear partial differential equations. *ESAIM: Mathematical Modelling and Numerical Analysis*, 41(3):575–605, 2007.
- [6] J. S. Hesthaven, G. Rozza, B. Stamm, et al. *Certified reduced basis methods for parametrized partial differential equations*, volume 590. Springer, 2016.
- [7] S. Hijazi, G. Stabile, A. Mola, and G. Rozza. Data-driven pod-galerkin reduced order model for turbulent flows. *Journal of Computational Physics*, 416:109513, 2020.
- [8] C. Hoang, K. Chowdhary, K. Lee, and J. Ray. Projection-based model reduction of dynamical systems using space-time subspace and machine learning. *arXiv preprint arXiv:2102.03505*, 2021.
- [9] C. Hoang, K. Chowdhary, K. Lee, and J. Ray. Projection-based model reduction of dynamical systems using space-time subspace and machine learning. *arXiv preprint arXiv:2102.03505*, 2021.
- [10] C. Hoang, K. Chowdhary, K. Lee, and J. Ray. Projection-based model reduction of dynamical systems using space-time subspace and machine learning. *arXiv preprint arXiv:2102.03505*, 2021.
- [11] B. O. Koopman. Hamiltonian systems and transformation in hilbert space. *Proceedings of the national academy of sciences of the united states of america*, 17(5):315, 1931.
- [12] J. N. Kutz, S. L. Brunton, B. W. Brunton, and J. L. Proctor. *Dynamic mode decomposition: data-driven modeling of complex systems*. SIAM, 2016.
- [13] S. Le Clainche and J. M. Vega. Higher order dynamic mode decomposition. *SIAM Journal on Applied Dynamical Systems*, 16(2):882–925, 2017.
- [14] S. Le Clainche and J. M. Vega. Higher order dynamic mode decomposition to identify and extrapolate flow patterns. *Physics of Fluids*, 29(8):084102, 2017.
- [15] S. Le Clainche, J. M. Vega, and J. Soria. Higher order dynamic mode decomposition of noisy experimental data: The flow structure of a zero-net-mass-flux jet. *Experimental Thermal and Fluid Science*, 88:336–353, 2017.
- [16] R. Penrose. On best approximate solutions of linear matrix equations. In *Mathematical Proceedings of the Cambridge Philosophical Society*, volume 52, pages 17–19. Cambridge University Press, 1956.
- [17] A. Quarteroni, R. Sacco, and F. Saleri. *Numerical mathematics*, volume 37. Springer Science & Business Media, 2010.
- [18] T. Sayadi, P. J. Schmid, F. Richecoeur, and D. Durox. Parametrized data-driven decomposition for bifurcation analysis, with application to thermo-acoustically unstable systems. *Physics of Fluids*, 27(3):037102, 2015.
- [19] M. Tezzele, N. Demo, M. Gadalla, A. Mola, and G. Rozza. Model order reduction by means of active subspaces and dynamic mode decomposition for parametric hull shape design hydrodynamics. In *Technology and Science for the Ships of the Future: Proceedings of NAV 2018: 19th International Conference on Ship & Maritime Research*, pages 569–576. IOS Press, 2018.
- [20] M. Tezzele, N. Demo, and G. Rozza. Shape optimization through proper orthogonal decomposition with interpolation and dynamic mode decomposition enhanced by active subspaces. In *VIII International Conference on Computational Methods in Marine Engineering*, 2019.
- [21] M. Tezzele, N. Demo, G. Stabile, A. Mola, and G. Rozza. Enhancing cfd predictions in shape design problems by model and parameter space reduction. *Advanced Modeling and Simulation in Engineering Sciences*, 7(1):40, Oct 2020.

- [22] C. K. Williams and C. E. Rasmussen. *Gaussian processes for machine learning*, volume 2. MIT press Cambridge, MA, 2006.